NO^+ formation pathways in dissociation of N_2O^+ ions at the $C^2\Sigma^+$ state revealed from threshold photoelectron–photoion coincidence velocity imaging

Xiaofeng Tang,[1] Mingli Niu,[1] Xiaoguo Zhou,[1,a)] Shilin Liu,[1] Fuyi Liu,[2] Xiaobin Shan,[2] and Liusi Sheng[2]

[1]*Hefei National Laboratory for Physical Sciences at the Microscale, Department of Chemical Physics, University of Science and Technology of China, Hefei, Anhui 230026, People's Republic of China*

[2]*National Synchrotron Radiation Laboratory, University of Science and Technology of China, Hefei, Anhui 230029, People's Republic of China*

(Received 21 October 2010; accepted 8 January 2011; published online 4 February 2011)

Using the novel threshold photoelectron–photoion coincidence (TPEPICO) velocity imaging technique, the dissociative photoionization of N_2O molecule via the $C^2\Sigma^+$ ionic state has been investigated. Four fragment ions, NO^+, N_2^+, O^+, and N^+, are observed, respectively, and the NO^+ and N^+ ions are always dominant in the whole excitation energy range of the $C^2\Sigma^+$ ionic state. Subsequently, the TPEPICO three-dimensional time-sliced velocity images of NO^+ dissociated from the vibrational state-selected $N_2O^+(C^2\Sigma^+)$ ions have been recorded. Thus the kinetic and internal energy distributions of the NO^+ fragments have been obtained directly as the bimodal distributions, suggesting that the NO^+ fragments are formed via both $NO^+(X^1\Sigma^+) + N(^2P)$ and $NO^+(X^1\Sigma^+) + N(^2D)$ dissociation channels. Almost the same vibrational population reversions are identified for both dissociation pathways. Interestingly, the obtained branching ratios of the two channels exhibit some dependence on the excited vibrational mode for $N_2O^+(C^2\Sigma^+)$, in which the excited asymmetrical stretching potentially promotes dissociation possibility along the $NO^+(X^1\Sigma^+) + N(^2D)$ pathway. In addition, the measured anisotropic parameters of NO^+ are close to 0.5, indicating that the $C^2\Sigma^+$ state of N_2O^+ is fully predissociative, indeed, with a tendency of parallel dissociation, and therefore, the corresponding predissociation mechanisms for the $N_2O^+(C^2\Sigma^+)$ ions are depicted. © *2011 American Institute of Physics*. [doi:10.1063/1.3549130]

I. INTRODUCTION

As one of the most important chemical processes in the upper ionosphere, the ion–molecule reaction, $O^+ + N_2 \rightarrow NO^+ + N$, has been explored extensively.[1–5] In this reaction, the N_2O^+ molecular ion plays an essential role as a significant intermediate in its reaction mechanism. Therefore, numerous theoretical[1,3,6,7] and experimental studies[6–35] have been performed on its structure and dynamics.

N_2O is a typical asymmetrical molecule with the valence electronic configuration of $(1\sigma)^2(2\sigma)^2(3\sigma)^2(4\sigma)^2(5\sigma)^2(6\sigma)^2(1\pi)^4(7\sigma)^2(2\pi)^4$. Ejection of an electron from the outer orbitals leads to the formation of $X^2\Pi$, $A^2\Sigma^+$, $B^2\Pi$, and $C^2\Sigma^+$ states of N_2O^+, respectively.[6,8] Many experimental techniques, such as He I photoelectron spectroscopy (PES),[8–12] threshold photoelectron spectroscopy (TPES),[13–16] and pulsed field ionization photoelectron spectroscopy (PFI-PES),[17–19] together with some theoretical investigations[1,3,6,20,21] have provided the detailed information of the vibronic structures of N_2O^+. Consequently, the dissociation of N_2O^+ at the lower electronic states has been explored by various experimental methods including electron ionization,[22–24] photofragment excitation spectroscopy,[25–28] photoionization mass spectroscopy,[29,30] fast-ion beam laser spectroscopy,[31,32] photoelectron-photoion coincidence (PEPICO),[33,34] and threshold photoelectron–photoion coincidence (TPEPICO) spectroscopy.[13–16]

The previous studies have clarified that the $X^2\Pi$ ground state of N_2O^+ is bound with a linear geometry. Many complex spectroscopic features, e.g., spin–orbit coupling, Fermi resonance, and Renner–Teller interaction associated with the v_2^+ bending excitation in the $X^2\Pi$ state, have been revealed.[19] The first electronically excited state, $A^2\Sigma^+$, can decay via fluorescence and/or predissoication.[13,15,33,34] Briefly, N_2O^+ ions at the vibrational levels of $A^2\Sigma^+$ state can predissociate to form NO^+ and N fragments, except for the ground vibrational state. Recently, a systematic spectroscopic and dissociation dynamic studies have been done for the $N_2O^+(A^2\Sigma^+)$ ions at the various vibrational levels.[25–28] The strong Fermi resonance couplings have been found between the v_1^+ (symmetrical stretch), v_2^+ (bending), and v_3^+ (asymmetrical stretch) vibrational modes in the $A^2\Sigma^+$ state.[25,26] More interestingly, a channel switching effect has been observed in a special excitation energy region between two energetically accessible dissociation limits, $NO^+(X^1\Sigma^+) + N(^4S)$ and $NO^+(X^1\Sigma^+) + N(^2D)$.[26,27] Based on the measured kinetic energy released distribution (KERD) of NO^+ fragment by velocity map imaging (VMI), three dissociation pathways for the $N_2O^+(A^2\Sigma^+)$ ions have been proposed, which are as follows:[28]

a)Author to whom correspondence should be addressed. Electronic mail: xzhou@ustc.edu.cn.

$$N_2O^+(A^2\Sigma^+)\begin{cases}\xrightarrow{\text{spin-orbit}} N_2O^+(1^4\Pi,\text{bent}) \rightarrow \begin{cases} N_2O^+(1^4\Sigma^-) \rightarrow NO^+(X^1\Sigma^+) + N(^4S) \\ N_2O^+(^2\Sigma^-/^2\Delta) \rightarrow NO^+(X^1\Sigma^+) + N(^2D)\,. \end{cases} \\ \xrightarrow{\text{vibronic}} N_2O^+(X^2\Pi,\text{linear}) \rightarrow NO^+(X^1\Sigma^+) + N(^2D)\end{cases} \quad (1)$$

Compared with the $X^2\Pi$ and $A^2\Sigma^+$ states, the higher electronically excited states of N_2O^+, $B^2\Pi$, and $C^2\Sigma^+$ have not been investigated sufficiently, although both the $B^2\Pi$ and $C^2\Sigma^+$ states are well-known to be predissociative. The PES and PFI-PES for the $N_2O^+(B^2\Pi)$ state display a complex spectral structure with a long series of broad peaks superimposed over a continuous background, and no simple vibrational progressions can be assigned.[19,21] For the $B^2\Pi$ state, although the NO^+, N_2^+, and O^+ fragments are energetically allowed, the previous TPEPICO and PEPICO experiments[13,34] show that NO^+ is the dominant fragment, and N_2^+ can also be formed with a smaller abundance, while the intensity of O^+ is nearly negligible. Moreover, the kinetic energy distribution of NO^+ shows strongly bimodal, corresponding to the $NO^+(X^1\Sigma^+) + N(^2D)$ and $NO^+(X^1\Sigma^+) + N(^2P)$ channels, respectively.[34] Earlier theoretical calculations on potential energy curves of the lower electronic states of N_2O^+ surmise that interactions between the $B^2\Pi$ and $1^4\Pi$ (or $D^2\Pi$) states in the near energy region cause predissociation of the $B^2\Pi$ state.[22,23] The later complete active space self-consistent field calculation[3] further reveals that the $B^2\Pi$ state correlates adiabatically with the $NO^+(X^1\Sigma^+) + N(^2P)$ dissociation limit, and it can readily dissociate via the conical intersection of the $^2A''$ component of $B^2\Pi$ with the $^2\Sigma^-$ or $^2\Delta$ states.

Within the energy range of 19.9–21.0 eV, the vibrational structure of the $C^2\Sigma^+$ state has been measured by various experimental methods, e.g., He I PES,[8–11] TPES,[13,16] and PFI-PES.[19] Similar to that of the $A^2\Sigma^+$ state, the dominate resonance structures are observed as the (0,0,0), (1,0,0), and (0,0,1) vibronic bands for the $C^2\Sigma^+$ state, with a very weak band (0,1,0) as excitation of bending. Here, the numbers in parentheses correspond to vibrational quanta for the ν_1^+, ν_2^+, and ν_3^+ modes, respectively. Therefore, the $N_2O^+(C^2\Sigma^+)$ ion has a quasilinear geometry as the $A^2\Sigma^+$ state. Since many dissociation limits can be achieved within the excitation energy range of the $C^2\Sigma^+$ state,[6,13] as shown in Table I, the NO^+, N_2^+, O^+, and N^+ fragments can be formed from the dissociation of the $N_2O^+(C^2\Sigma^+)$ ion. The branching ratios of fragment ions have been measured by Kinmond *et al.* with PEPICO approach.[34] Using the higher energy-resolution TPEPICO technique, Nenner *et al.*[13] and Chiang and Ma[16] have individually remeasured the branching ratios and average kinetic energy released from the major fragment ions in dissociation of the $N_2O^+(C^2\Sigma^+)$ ion. It should be emphasized that the average kinetic energy distribution of fragment ions in these studies have been determined from widths of the corresponding time-of-flight (TOF) profiles, which are, indeed, too rough to discuss dissociation dynamics in detail. Recently, the dissociative photoionization (DPI) of N_2O via the $C^2\Sigma^+$ state has been studied by the vector correlation method.[35] Its most attention has been paid on molecular frame photoelectron angular distributions in the photoionization process, and the lifetime of $C^2\Sigma^+$ prior to dissociation has been estimated to be about 2 ps. However, the dissociation information is not very clear due to its poor energy resolution, especially for the dissociation mechanism and branching ratios of different dissociation channels.

Although extensive experimental studies have been performed previously for the $N_2O^+(C^2\Sigma^+)$ ion, the dissociation mechanism, the kinetic energy and internal state distributions of fragments, and angular distributions of fragment ions are still not clarified. Especially, the kinetic energy released from the fragment measured by simulating the TOF profile in previous studies is a low resolution method, indeed, for obtaining the state distribution of fragment, as mentioned above, and thereby, the detailed information of dissociation dynamics may be buried. Moreover, a special attention should be paid to comparing the NO^+ formation pathways in dissociation of N_2O^+ ions at the $A^2\Sigma^+$ with $C^2\Sigma^+$ states, since both the electronic states have the same symmetry and very similar linear geometries, even the vibrational frequencies of both the states are close in a certain degree.

In this work, a reinvestigation on the DPI of the N_2O molecule via the $C^2\Sigma^+$ ionic state has been performed using a recently developed TPEPICO velocity imaging technique.[36] By using the ion velocity imaging of high energy resolution, the velocity distribution of NO^+ fragments is measured. Based on the velocity distributions, the NO^+ formation pathways are obtained, and the corresponding vibrational state distributions of NO^+ are identified for every dissociation channels. Furthermore, the branching ratios of possible dissociation channels are observed, depending on the excitation vibrational modes of $C^2\Sigma^+$ from the recorded images of NO^+ dissociating from the vibrational state-selected $N_2O^+(C^2\Sigma^+)$ ions. Therefore, the potential predissociation mechanism of the $N_2O^+(C^2\Sigma^+)$ ion will be finally proposed to interpret our observations, although the detailed potential energy surfaces of $C^2\Sigma^+$ are not clear.

II. EXPERIMENTAL

The present TPEPICO velocity imaging apparatus combines the TPEPICO (Refs. 37 and 38) and VMI (Ref. 39) techniques to detect both threshold photoelectrons and photoions in experiments. All experiments have been performed at the U14-A beam line of the National Synchrotron Radiation Laboratory (Hefei, China). The apparatus and the beam line have been described in detail previously,[36,40] and thus only a brief introduction is given here.

The monochromatic undulator synchrotron radiation (SR) is used to photoionize a molecule. With 80 μm widths of

TABLE I. Potential dissociation limits of N_2O^+ ion in the excitation energy range of 19.9–20.7 eV.

Energy (eV)	Fragments	Corresponding states of N_2O^+
14.19	$NO^+(X^1\Sigma^+) + N(^4S)$	$^4\Sigma^-$
16.57	$NO^+(X^1\Sigma^+) + N(^2D)$	$^2\Sigma^-$, $^2\Pi$, $^2\Delta$
17.77	$NO^+(X^1\Sigma^+) + N(^2P)$	$^2\Sigma^+$, $^2\Pi$
20.66	$NO^+(a^3\Sigma^+) + N(^4S)$	$^{2,4,6}\Sigma^-$
17.25	$N_2^+(X^2\Sigma_g^+) + O(^3P)$	$^{2,4}\Sigma^-$, $^{2,4}\Pi$
18.39	$N_2^+(A^2\Pi_u) + O(^3P)$	$^{2,4}\Pi$, $^{2,4}\Delta$, $^{2,4}\Sigma^+$, $^{2,4}\Sigma^-$
19.22	$N_2^+(X^2\Sigma_g^+) + O(^1D)$	$^2\Sigma^+$, $^2\Pi$, $^2\Delta$
20.35	$N_2^+(A^2\Pi_u) + O(^1D)$	$^2\Sigma^-$, $^2\Sigma^+$, $2(^2\Pi)$, $^2\Delta$, $^2\Phi$
20.48	$N_2^+(B^2\Sigma_u^+) + O(^3P)$	$^2\Sigma^-$, $^2\Pi$
15.29	$O^+(^4S) + N_2(X^1\Sigma_g^+)$	$^4\Sigma^-$
18.61	$O^+(^2D) + N_2(X^1\Sigma_g^+)$	$^2\Sigma^-$, $^2\Pi$, $^2\Delta$
20.31	$O^+(^2P) + N_2(X^1\Sigma_g^+)$	$^2\Sigma^+$, $^2\Pi$
19.46	$N^+(^3P) + NO(X^2\Pi)$	$^{2,4}\Sigma^+$, $^{2,4}\Sigma^-$, $^{2,4}\Pi$, $^{2,4}\Delta$

the entrance and exit slits of monochromator, the energy resolution of SR is about 2000 of $E/\Delta E$. In present experiments, the absolute photon energy has been calibrated with the well-known ionization energies of inert gases, and the higher order harmonic radiation of the undulator has been eliminated by a gas filter filled with neon prior to enter the photoionization chamber.

N_2O sample (99.9%) is used without any further purification in experiments. A continuous supersonic molecular beam (MB) of pure N_2O gas is introduced into photoionization region through a homemade 30 μm diameter nozzle with a stagnation pressure of 1.1 atm, collimated by a 0.5 mm diameter skimmer, and then intersected by SR at 10 cm downstream from the nozzle. The source and ionization chambers of the apparatus are pumped, respectively, by 1800 and 1600 l/s turbomolecular pumps, and thus the typical backing pressures are 2×10^{-3} and 4×10^{-5} Pa with the molecular beam on.

Photoelectrons and photoions are collected through a special ion lens to map their velocity images simultaneously.[36] A 1 mm diameter aperture is placed in front of the electron detector to block most energetic electrons. Using the detected threshold photoelectrons as the start signals for measuring TOFs of ions, the coincident photoions are mapped through the VMI electric field and projected onto a dual microchannel plate (MCP) backed by a phosphor screen (Burle Industries, P20). A TE-cooling CCD detector (Andor, DU934N-BV) is used to record images on the screen. By applying a pulsed high voltage on MCP as the mass gate, the three-dimensional (3D) time-sliced image of ions can be obtained directly.[41] Moreover, the signal intensities of detected electrons and ions can be normalized using the photon flux from a silicon photodiode (International Radiation Detectors Inc., SXUV-100).

III. RESULTS AND DISCUSSION

A. TPES for $N_2O^+(C^2\Sigma^+)$

The present energy resolution of threshold photoelectron is about 9 meV [full width at half maximum (FWHM)] when the extraction electric field in the interaction region is 14 V/cm,[36] and thereby the vibronic structures of ion can be easily discerned. Figure 1 shows the measured TPES of $N_2O^+(C^2\Sigma^+)$ in the excitation energy range of 19.9–20.7 eV with an increment of 0.005 eV. The most spectral assignments are given as transitions from the ground $X^1\Sigma^+$ state of N_2O molecule, according to Chen *et al.*'s data,[19] e.g., the (1,0,0) band corresponds to the ionization transition of $N_2O^+(C^2\Sigma^+,1,0,0) \leftarrow N_2O(X^1\Sigma^+,0,0,0)$.

As shown in Table II, the energy positions and relative intensities of every resonance peaks in the present TPES agree very well with previous experiments.[16,19] Three most dominate resonance bands in the TPES are (0,0,0), (1,0,0), and (0,0,1), while the (0,1,0) bending band is very weak, indicating that the $C^2\Sigma^+$ state of N_2O^+ has a quasilinear geometry. Moreover, the relative intensities of the observed vibrational bands in the TPES of the $C^2\Sigma^+$ state are very similar to those of the $A^2\Sigma^+$ state, implying that the $C^2\Sigma^+$ and $A^2\Sigma^+$ states of N_2O^+ have almost the same geometry. The vibrational frequencies of these two electronic states are also close, e.g.,

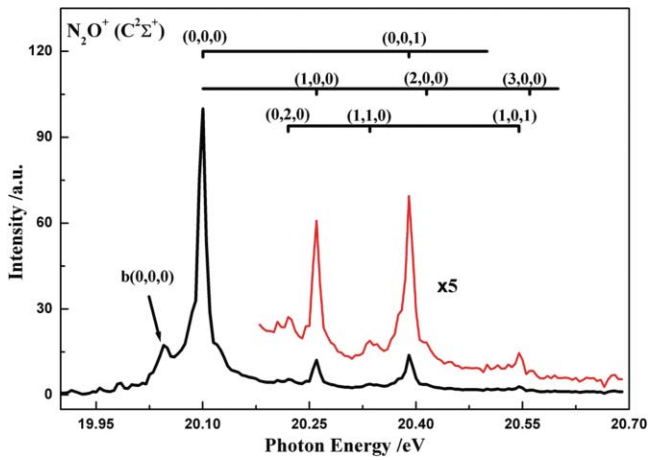

FIG. 1. Threshold photoelectron spectrum for N_2O in the excitation energy range of 19.9–20.7 eV with an increment of 0.005 eV. The vibrational progressions of the $C^2\Sigma^+$ state are assigned, according to Ref. 19.

TABLE II. Spectral assignments, ionization energies, and relative intensities of threshold photoelectron spectra of N_2O in the excitation energy range of 19.9–20.7 eV.

	Ionization energy (eV)				Relative intensity		
Assignment	Present	Ref. 13	Ref. 16	Ref. 19	Present	Ref. 11	Ref. 19
b(0,0,0)	20.045		20.05	20.0443	17.3		1.8
C(0,0,0)	20.100	20.11	20.10	20.1047	100	100	100
C(1,0,0)	20.260	20.27	20.26	20.2598	12.2	13.5	7.3
C(0,0,1)	20.390	20.40	20.39	20.3899	13.9	18.7	8.5

$v_1^+ = 1346\ cm^{-1}$, $v_2^+ = 611\ cm^{-1}$, and $v_3^+ = 2450\ cm^{-1}$ for the $A^2\Sigma^+$ state, while $v_1^+ = 1251\ cm^{-1}$, $v_2^+ = 482\ cm^{-1}$, and $v_3^+ = 2300\ cm^{-1}$ for the $C^2\Sigma^+$ state.[19] Therefore, the shapes of potential energy curves for these two ionic states should be very similar, especially in the region of the lower vibrational states.

In addition to the three dominate bands, a shoulder band at 20.045 eV has been observed and tentatively identified as b(0,0,0) level in Chiang and Ma's assignment[16] and reassigned as the $1_0{}^1 2_3{}^0$ band of $C^2\Sigma^+$ in Chen *et al.*'s study.[19] Although almost all resonance structures in present TPES can be assigned definitely as Chen *et al.*'s assignment due to its much higher energy resolution, even for those concomitant weak bands in Fig. 1, we prefer to use Chiang and Ma's assignment for this shoulder band. As discussed in Chiang and Ma's work,[16] this shoulder band cannot be assigned as a spectral component of the $C^2\Sigma^+$ state, based on the fact that it does not belong to the Rydberg series converging to the $C^2\Sigma^+$ state in photoionization efficiency curves. Additionally, only NO^+ and $N_2{}^+$ fragments have been observed with visible intensity in the TPEPICO TOF mass spectrum for this sub-band, which is essentially different with the measured time-of-flight mass spectra (TOF-MS) for other vibrational bands of the $C^2\Sigma^+$ state.[16] However, the velocity imaging has not been applied for this shoulder band in the present study due to its lower intensity.

B. TPEPICO TOF-MS of N_2O^+ ($C^2\Sigma^{+)}$

As shown in Table I, many dissociation limits for the $C^2\Sigma^+$ state can be reached in the present excitation energy range, and the corresponding ionic fragments are NO^+, N^+, O^+, and $N_2{}^+$. When the excitation energies are fixed, respectively, at the b(0,0,0), C(0,0,0), C(1,0,0), and C(0,0,1) bands, the measured TPEPICO TOF-MS are presented in Fig. 2, where the four ionic fragments can be clearly discerned, and the relative intensities are observed very similar to previous results.[16,34] With the 14 V/cm extraction field in the photoionization region, the width of TOF profile for parent ion is about 17 ns (FWHM) in this spectrometer,[36] while those of the fragment ions are broaden due to the released kinetic energy in dissociation and thereby the mass resolution is decreased. As only fragment ions have been observed, the $C^2\Sigma^+$ state of N_2O^+ is, indeed, fully predissociative.

In Fig. 2, the TOF peaks centered at 5.88 and 6.29 μs are symmetrically broaden and assigned to the N^+ and O^+ fragment ions, respectively. Another broadened TOF profile at around 8.6 μs is obviously unsymmetrical, which seems coming from overlapping of two TOF peaks. Using two Gaussian functions to fit the TOF profile, two TOF peaks are identified to be centered at 8.33 and 8.63 μs and correspond to the $N_2{}^+$ and NO^+ ions, respectively. By integrating areas of the Gaussian profiles, the branching ratios of fragment ions can be obtained and presented in Table III, as well with the previous results.[16,34] Although there are some extent differences of intensity ratios among the present and previous results, the tendencies of all the branching ratios are very similar. The NO^+ and N^+ ions are always dominant in dissociation processes of the C(0,0,0), C(1,0,0), and C(0,0,1) bands, while the $N_2{}^+ + NO$ and $O^+ + N_2$ dissociation channels are minor. For the b(0,0,0) state, only NO^+ fragment has been observed with visible intensity in the TPEPICO TOF-MS, which is consistent with the previous conclusions.[16] Since the major aim of present study is focused to vibrational state-selected dissociation of the $C^2\Sigma^+$ state, the corresponding data of the b(0,0,0) state are not involved in Table III.

C. Kinetic energy distribution of NO^+ fragments

Through simulating the measured TOF profiles, the released average kinetic energies of fragment ions can be estimated.[13,16,42–44] However, the energy resolution of the simulated results is so poor that the detailed kinetic and internal energy information in dissociation cannot be discerned. Moreover, the angular distribution of fragment ions cannot be obtained directly from the simple simulation of the TOF profiles. Similarly, the previous vector correlation measurement[35] also has a disadvantage of poor energy resolution in the investigation of the DPI process of the $N_2O^+(C^2\Sigma^+)$ ions. Therefore, some dedicated dissociation information could be buried in the previous experiments.

Actually, the present TPEPICO velocity imaging measurements can provide relative high energy resolutions for both photoelectrons and photoions,[36] and thereby the kinetic energy distribution of fragment ions can be accurately obtained from their images [the kinetic energy resolution of ion images can be better than 3% (Ref. 36)]. In addition, the angular distribution of fragment ions will be obtained simultaneously from the images. Therefore, the present imaging

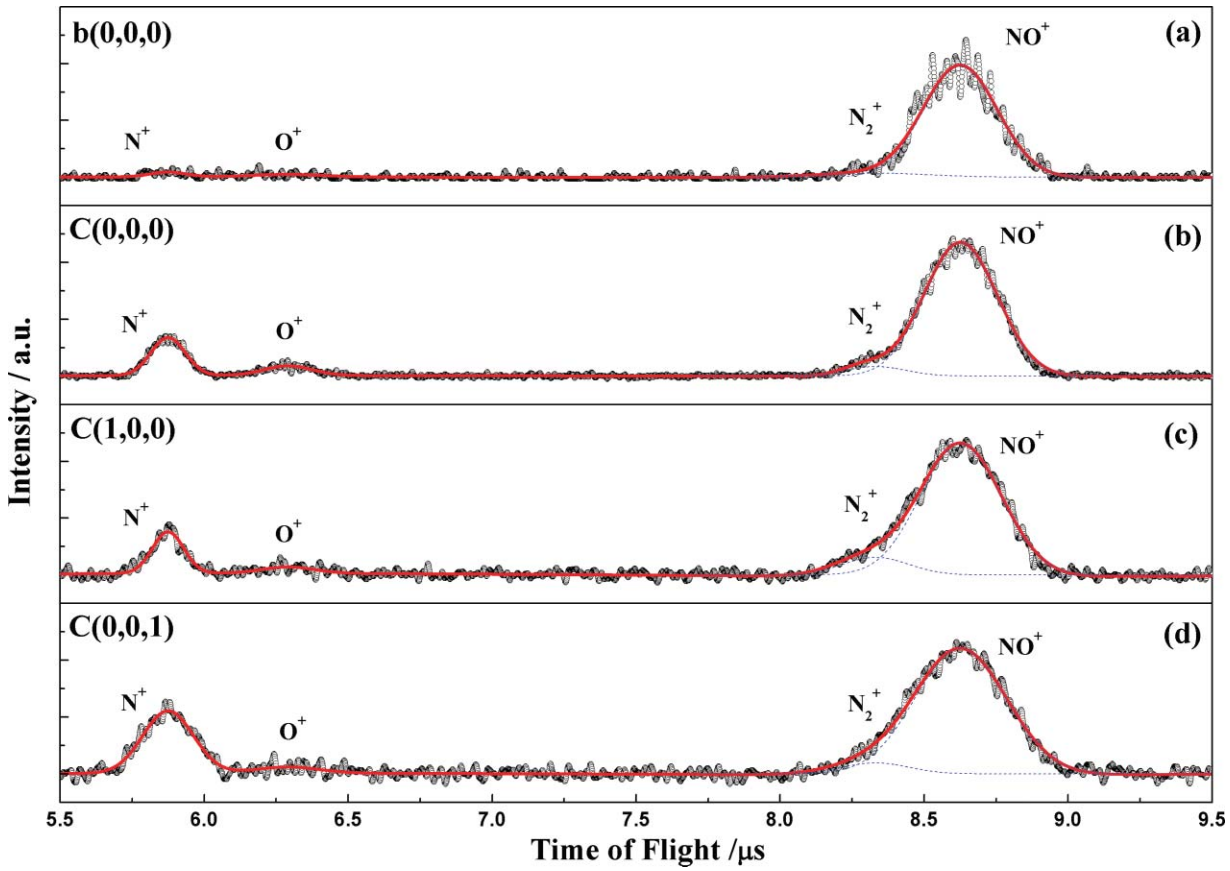

FIG. 2. Vibrational state-selected TPEPICO TOF mass spectra for the DPI process of N_2O. (a) b(0,0,0) state at 20.045 eV; (b) C(0,0,0) state at 20.100 eV; (c) C(1,0,0) state at 20.260 eV; (d) C(0,0,1) state at 20.390 eV.

experiments will provide much more detailed information in the DPI process.

Based on the TOF-MS of $N_2O^+(C^2\Sigma^+)$ in Fig. 2, the corresponding TPEPICO velocity images of NO^+ fragment ions have been recorded with a 80 ns duration mass gate, when threshold photoelectrons are used as the start to record TOF of ions. Since the false coincidence ions (mainly N_2O^+) constitute the background in TPEPICO TOF-MS as the nonzero baseline, their contributions are also partially recorded in the raw TPEPICO images of the NO^+ fragment, which are mostly corresponding to a bright spot close to the center. Through subtracting image of the false coincident ions, the real TPEPICO velocity image can be acquired and most influences of false coincidence events are eliminated. In addition, due to the center-of-mass speed of MB, all the ion images are recorded slightly eccentric from the center of CCD along the beam direction.[36] Moreover, according to the perpendicular configuration between the MB and the ion flight directions, the velocity spread of MB will inevitably contaminate images along the MB direction. Therefore, the real ion images need to be handled prior to extracting the speed and angular distribution, through a multistep data disposure scheme including quadrant symmetrization and deconvolution, and the detailed description is introduced in the supplementary material.[45] As a result, the 3D time-sliced velocity images of NO^+ dissociated from various vibrational states, e.g., (0,0,0), (1,0,0), and (0,0,1) of $N_2O^+(C^2\Sigma^+)$, are presented in Fig. 3.

TABLE III. Branching ratios of fragment ions dissociated from the $N_2O^+(C^2\Sigma^+)$ ion.

	Branching ratios (%)								
	(000)			(100)			(001)		
Dissociation channel	Present	Ref. 16	Ref. 34	Present	Ref. 16	Ref. 34	Present	Ref. 16	Ref. 34
$NO^+ + N$	81	67 ± 1	74 ± 1	80	70 ± 1	70 ± 1	73	63 ± 1	69 ± 1
$N_2^+ + O$	4	8 ± 1	10 ± 2	8	11 ± 1	16 ± 3	4	6 ± 1	9 ± 4
$O^+ + N_2$	4	5 ± 1	4 ± 2	2	4 ± 1	3 ± 4	3	2 ± 1	3 ± 5
$N^+ + NO$	11	20 ± 1	12 ± 2	10	15 ± 1	9 ± 4	20	29 ± 1	18 ± 4

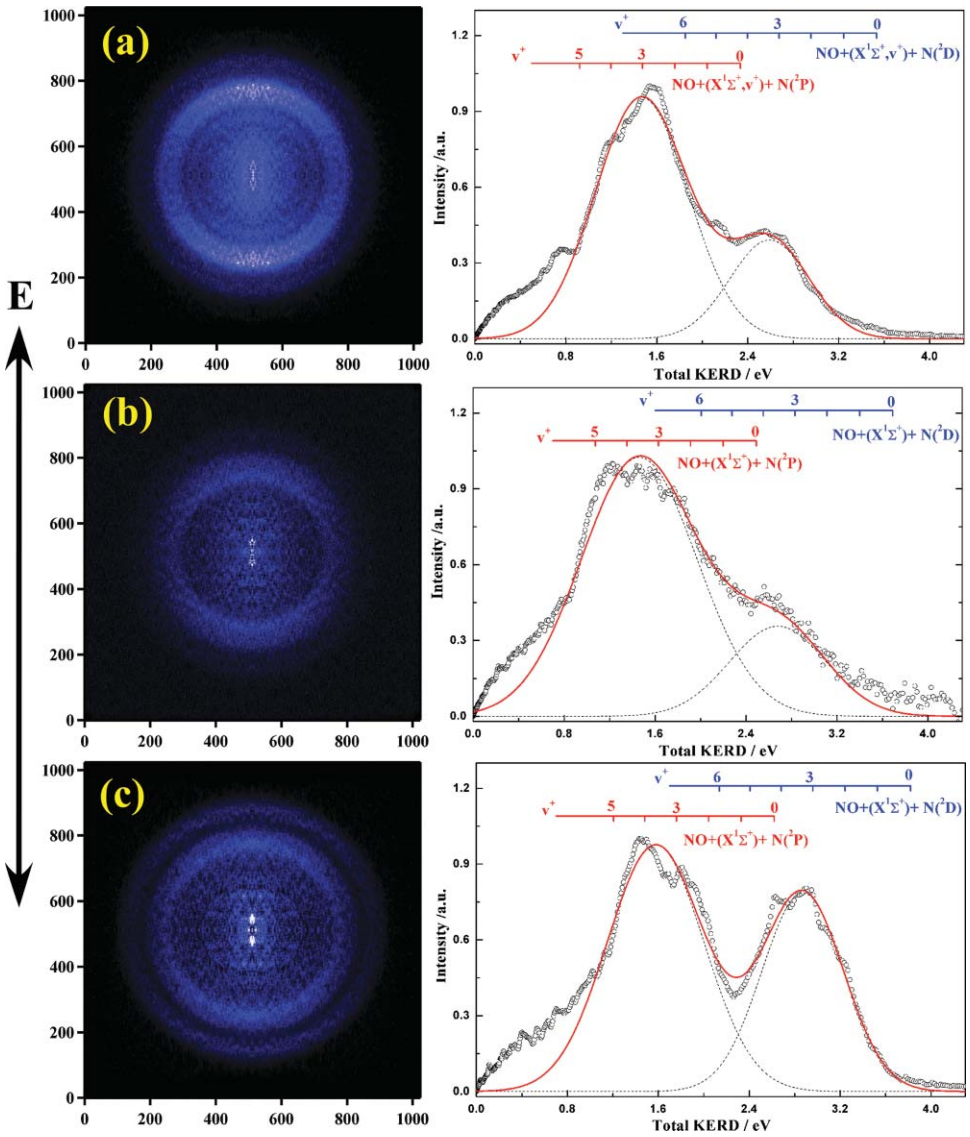

FIG. 3. 3D time-sliced coincidence images of NO^+ and total kinetic energy released distributions at different vibronic levels of $N_2O^+(C^2\Sigma^+)$ state. The electric vector E of synchrotron radiation is noted as the vertical direction of the image plane, where (a)–(c) are recorded at 20.100, 20.260, and 20.390 eV, respectively, and corresponding to the C(0,0,0), C(1,0,0), and C(0,0,1) vibronic levels. Least-squares fitting of the total KERD curves with two Gaussian profiles are plotted with the solid line.

Frankly, due to nonuniformity of measurements of coincidence and false coincidence ions, a few residual contributions of the false coincidence ions still exist in all images of Fig. 3, most of which are close to center of images and contribute intensities of $E_T < 0.8$ eV in the KERD curves of Fig. 3. Since they can cause some uncertainties in the lower KERD, we will not discuss these distributions. Besides the centric parts in all the images, two main rings are observed clearly with different intensity ratios. By accumulating the intensities of NO^+ at different velocities in images, the speed or kinetic energy distributions of NO^+ ions in the DPI process are acquired directly. As the total linear momentum and energy of fragments are conserved in the center-of-mass frame, the total KERD in dissociation process can be obtained subsequently and shown at the right side of Fig. 3. Obviously, two major vibrational distribution peaks are observed in all the total KERD curves, which are seriously different from the previous conclusions of the vector correlation[35] and PEPICO (Ref. 34) measurements where only one type distributions were obtained. Due to the poor energy resolution of the vector correlation and simulating TOF profiles in the PEPICO measurements, the present results should be more reliable. Moreover, the inner ring is kept with the higher intensity than the outer one, whatever the $\nu_1{}^+$ or $\nu_3{}^+$ vibrational mode of the $C^2\Sigma^+$ state is excited.

The assignments of NO^+ fragment kinetic energy distribution in terms of internal states are based on the conservations of energy and momentum in the dissociation process. From the point of energy conversation, the internal energy of NO^+ fragment, E_{int}, and the total released kinetic energy for both NO^+ and N fragments, E_T, have the following relation,

$$h\nu - D_0 = E_{int} + E_T, \tag{2}$$

where $h\nu$ is the excitation photon energy, and D_0 is the dissociation limit for a specific channel. The E_T can be obtained from momentum conservation,

$$M_{NO^+} V_{NO^+} = M_N V_N, \tag{3}$$

and

$$E_T = \tfrac{1}{2} M_{NO^+} V_{NO^+}^2 + \tfrac{1}{2} M_N V_N^2, \tag{4}$$

where M_{NO^+}, M_N, V_{NO^+}, and V_N represent the masses and velocities of the NO^+ and N fragments, respectively. Taking the dissociation limit $D_0 = 16.57$ eV for the $NO^+(X^1\Sigma^+)$ + $N(^2D)$ channel and $D_0 = 17.77$ eV for the $NO^+(X^1\Sigma^+)$ + $N(^2P)$ channel in Table I, as well as the vibrational frequency $\nu^+ = 2376.42$ cm^{-1} (Ref. 46) and anharmonicity parameter $\omega_e X_e = 16.262$ cm^{-1} (Ref. 47) of NO^+, the possible vibrational state population of NO^+ fragment dissociated from the vibrational state-selected $N_2O^+(C^2\Sigma^+)$ ions can be assigned and shown at the right side of Fig. 3 as well. According to the large energy difference between the two dissociation limits, it is straightforward to assign the lower kinetic energy distribution in the total KERD curves as the $NO^+(X^1\Sigma^+)$ + $N(^2P)$ dissociation channel, while the higher kinetic energy distribution is assigned as the $NO^+(X^1\Sigma^+)$ + $N(^2D)$ dissociation channel. Seen from Fig. 3 [especially Fig. 3(c)], the two distributions show very similar quasi-Gaussian profiles.

It should be noted that no NO^+ ion corresponding to E_T of higher than 3.8 eV has been observed in all images of Fig. 3, and the corresponding TOF profiles of NO^+ in Fig. 2 are not dramatically spread too. Therefore, the branching ratio of the lowest dissociation channel to produce $NO^+(X^1\Sigma^+)$ and $N(^4S)$ fragments is insignificant in the present excitation energy range. Thus, the unique formation pathway for the $NO^+(X^1\Sigma^+)$ corresponding to E_T of more than 2.5 eV is along the $NO^+(X^1\Sigma^+)$ + $N(^2D)$ dissociation channel. Although individual vibrational state of NO^+ fragment cannot be identified clearly, the corresponding state distributions show an occurrence of vibrational population reversion. As assignments shown in Fig. 3, the maximum population possibilities of the $NO^+(X^1\Sigma^+,v^+)$ fragment are centering at $v^+ = 3$ for the $N_2O^+(C^2\Sigma^+,0,0,0)$ state. With the vibrational excitation of the $C^2\Sigma^+$ state, the most dominant populated vibrational states of the $NO^+(X^1\Sigma^+)$ fragment are slightly changed to $v^+ = 4$ for the $N_2O^+(C^2\Sigma^+,1,0,0)$ and $N_2O^+(C^2\Sigma^+,0,0,1)$ states. On the other hand, along the other dissociation channel of $NO^+(X^1\Sigma^+)$ + $N(^2P)$, the $N_2O^+(C^2\Sigma^+)$ ions can also produce $NO^+(X^1\Sigma^+,v^+)$ fragment, and the most dominant populated vibrational states of $NO^+(X^1\Sigma^+)$ are very similar to those of the $NO^+(X^1\Sigma^+)$ + $N(^2D)$ dissociation channel, e.g., the vibrational states of $NO^+(X^1\Sigma^+)$ fragment are mostly populated at $v^+ = 3$ for the $N_2O^+(C^2\Sigma^+,0,0,0)$ state, while they are gradually increased to $v^+ = 4$ for the $N_2O^+(C^2\Sigma^+,1,0,0)$ and $N_2O^+(C^2\Sigma^+,0,0,1)$ states.

D. Angular distribution of NO^+ fragments

From the images in Fig. 3, the angular distributions of NO^+ fragment ions dissociated from $N_2O^+(C^2\Sigma^+)$ vibrational states can be derived by integrating the images over a proper range of speed at each angle. Consequently, the anisotropy parameter β from different dissociation pathways can be calculated directly by simulating the angular distribution, $I(\theta)$, with the following formula,[48]

$$I(\theta) = (4\pi)^{-1}[1 + \beta P_2(\cos\theta)], \tag{5}$$

where θ is the angle between the recoil velocity of fragment and the electric field vector E of excitation light, and $P_2(\cos\theta)$ is the second-order Legendre polynomial. As a representative, both the experimental and fitted angular distributions of NO^+ fragment dissociated from $N_2O^+(C^2\Sigma^+,0,0,0)$ ions are presented in the inserted panel of Fig. 4, where the integrating range is chosen as $NO^+(X^1\Sigma^+, v^+ = 3)$ produced through the $NO^+(X^1\Sigma^+)$ + $N(^2P)$ dissociation channel. Seen from the simulated distributions with two Gaussian profiles in Fig. 3, the other dissociation channel of $NO^+(X^1\Sigma^+)$ + $N(^2D)$ has a negligible contribution to distribution intensity of $NO^+(X^1\Sigma^+,v^+ = 3)$ mentioned above, thereby the fitted β value represents the angular distribution of the $NO^+(X^1\Sigma^+)$ + $N(^2P)$ dissociation channel. Therefore, the obtained β for NO^+ fragments from different dissociation channels and various vibrational bands of $C^2\Sigma^+$ are summarized in Fig. 4. Obviously, all the anisotropic parameters are near 0.5, indicating that dissociation of the $N_2O^+(C^2\Sigma^+)$ ion has a tendency of parallel dissociation. These angular distributions of NO^+ fragments confirm that the $C^2\Sigma^+$ state of N_2O^+ is rapidly predissociative. As the previous spatial analysis of the (V_{NO^+}, V_e, P) vector correlation showed,[35] the β of NO^+ fragment was measured as 0.5 at 20.9 eV and a dominant parallel character of the transition was suggested, which is consistent with our conclusion. Moreover, a molecular frame forward–backward asymmetry of fragment angular distribution observed in experiment[35] indicated that electrons were emitted along the molecular axis in the direction of the N fragment, and hence, the $N_2O(X^1\Sigma^+)$ to $N_2O^+(C^2\Sigma^+)$ photoionization transition is dominantly contributed by a $d\sigma$ wave function for the parallel transition.

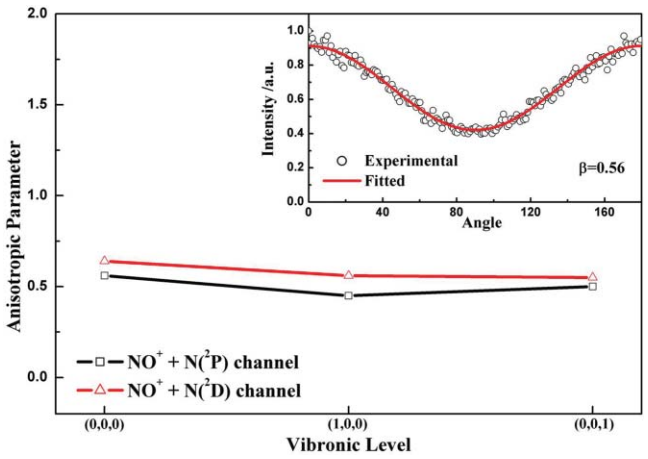

FIG. 4. Anisotropic parameters of dissociation from the vibrational state-selected $N_2O^+(C^2\Sigma^+)$ ions, where the symbol lines with triangles and squares are corresponding to the $NO^+(X^1\Sigma^+)$ + $N(^2D)$ and $NO^+(X^1\Sigma^+)$ + $N(^2P)$ dissociation channels, respectively. The experimental and fitted angular distributions of $NO^+(X^1\Sigma^+,v^+ = 3)$ fragments dissociated through the $NO^+(X^1\Sigma^+)$ + $N(^2P)$ dissociation channel from $N_2O^+(C^2\Sigma^+,0,0,0)$ ions are presented in the inserted figure, where the open circles represent experimental data and the solid line is the fitted result.

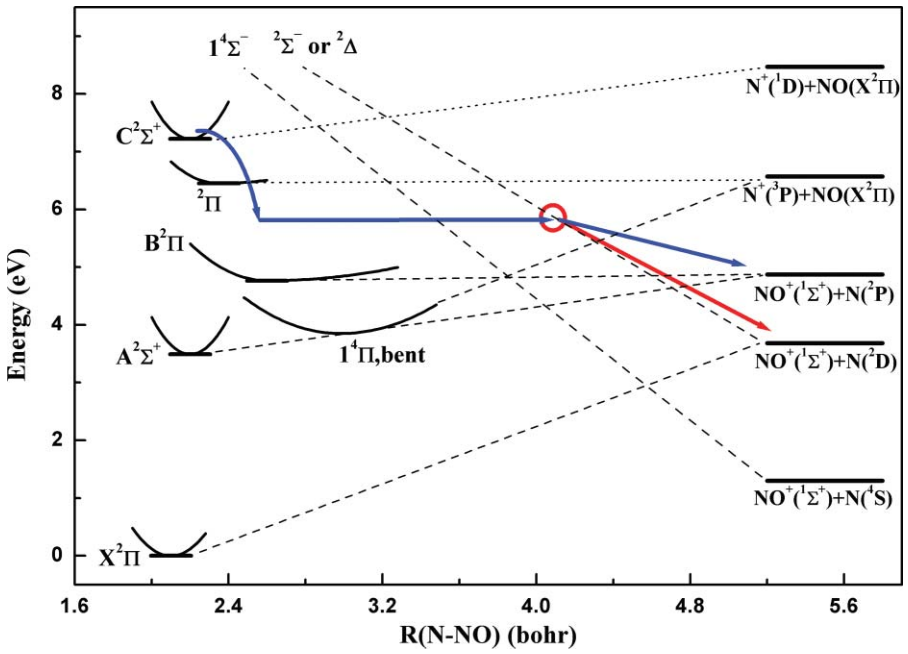

FIG. 5. Schematic diagram of adiabatic correlation for the low-lying electronic states of N_2O^+. The curve with the arrow represents a predissociation mechanism of the $C^2\Sigma^+$ state to produce $NO^+(X^1\Sigma^+)$ and $N(^2P)$ fragments, while the cycle notes the crossing from the $B^2\Pi$ state to $^2\Sigma^-$ (or $^2\Delta$) state, and the bottom curve with the arrow shows the indirect predissociation process via $B^2\Pi$ to form $NO^+(X^1\Sigma^+)$ and $N(^2D)$.

In addition, the magnitudes of anisotropic parameters do not change with the vibrational modes and dissociation channels for the $C^2\Sigma^+$ state, as shown in Fig. 4. This independent relationship indicates that the rate-determining steps of dissociation processes are probably the same for both dissociation pathways, and the very similar internal state distributions of NO^+ for both dissociation channels also imply this conclusion.

E. Predissociation mechanism of $N_2O^+(C^2\Sigma^+)$

According to the potential energy curves of low-lying electronic states of N_2O^+ ion, the dissociation limit $NO^+(X^1\Sigma^+) + N(^2P)$ correlates adiabatically with the predissociative $A^2\Sigma^+$ and $B^2\Pi$ states, while another dissociation limit $NO^+(X^1\Sigma^+) + N(^2D)$ links adiabatically with the repulsive $^2\Sigma^-$ and $^2\Delta$ states[3] and the $C^2\Sigma^+$ state links adiabatically with the $NO(X^2\Pi) + N^+(^1D)$ dissociation limit.[6] Besides these electronic states, the $D^2\Pi$ state potentially crosses the $C^2\Sigma^+$ state, and it is repulsive along the N–NO distance to form $NO(X^2\Pi)$ and $N^+(^3P)$ fragments.[3] The schematic diagram of adiabatic correlation for the low-lying electronic states of N_2O^+ is represented in Fig. 5. In addition, according to spectral structures of TPES and vibrational frequencies, the potential energy surface profile of $C^2\Sigma^+$ is suggested to be very similar to that of the $A^2\Sigma^+$ state, especially for the lower vibronic levels. Therefore, predissociation of $N_2O^+(C^2\Sigma^+)$ is expected to occur by interaction with the $C^2\Sigma^+$ and these nearby electronic states, e.g., $A^2\Sigma^+$, $B^2\Pi$, $D^2\Pi$, $^2\Sigma^-$, and $^2\Delta$ states.

First, the interaction between the $C^2\Sigma^+$ and repulsive $D^2\Pi$ states can make the $N_2O^+(C^2\Sigma^+)$ ion readily dissociate; however, the corresponding adiabatic ionic fragment should be $N^+(^3P)$.[3] Therefore, the present observed NO^+ fragments are impossible to be produced via the coupling between the $C^2\Sigma^+$ and $D^2\Pi$ states. Second, since the $A^2\Sigma^+$ and $C^2\Sigma^+$ states have the same symmetry and very similar geometry, the predissociation mechanisms of these two electronic states can be compared with each other. In the view of the kinetic energy distribution of the NO^+ fragment, the dominant dissociation mechanisms for the lower vibrational bands of the $A^2\Sigma^+$ and $C^2\Sigma^+$ states are entirely different. Most of the N_2O^+ $(A^2\Sigma^+)$ ions at the low vibronic levels dissociate to produce $NO^+(X^1\Sigma^+)$ and $N(^4S)$ through spin–orbit coupling with the $1^4\Pi$ bent state and subsequent crossing to $1^4\Sigma^-$ state prior to dissociation.[28] According to the fact that the $1^4\Pi$ and $1^4\Sigma^-$ states also probably cross with the $C^2\Sigma^+$ state, the similar predissociative pathway should be possible for the $C^2\Sigma^+$ state. However, the coupling between the $C^2\Sigma^+$ and $1^4\Pi$ states seems too weak to support this dissociation mechanism, since no NO^+ corresponding to the $N(^4S)$ fragment has been observed in the present experiment. Another possible dissociation pathway to produce NO^+ and $N(^2P)$ fragments from $N_2O^+(C^2\Sigma^+)$ is via interaction with the $A^2\Sigma^+$ state. However, as mentioned above, the $N(^4S)$ fragment should also be formed as the most dominant dissociative products of the $A^2\Sigma^+$ state, if $N_2O^+(C^2\Sigma^+)$ is crossed to the $A^2\Sigma^+$ state at the primary stage. This conclusion is obviously inconsistent with the experimental results.

Therefore, the interaction between the $B^2\Pi$ and $C^2\Sigma^+$ states is the unique mechanism to cause the predissociation of $N_2O^+(C^2\Sigma^+)$ to form $N(^2P)$ and $NO^+(X^1\Sigma^+)$ fragments. Specifically, the most possible way to form $N(^2P)$ and $NO^+(X^1\Sigma^+)$ fragments from the N_2O^+ $(C^2\Sigma^+)$ ions is a direct predissociation via the $B^2\Pi$ state, i.e., $N_2O^+(C^2\Sigma^+) \rightarrow N_2O^+(B^2\Pi) \rightarrow NO^+(X^1\Sigma^+) + N(^2P)$. Consequently, the $N(^2D)$ formation is caused by an indirect predissociation, i.e., $N_2O^+(C^2\Sigma^+) \rightarrow N_2O^+(B^2\Pi) \rightarrow$

$N_2O^+(^2\Sigma^-$ or $^2\Delta) \rightarrow NO^+(X^1\Sigma^+) + N(^2D)$. In summary, the observed NO^+ formation pathways in dissociation of $N_2O^+(C^2\Sigma^+)$ ions can be summarized as the following:

$$N_2O^+(C^2\Sigma^+) \rightarrow N_2O^+(B^2\Pi) \begin{cases} \rightarrow NO^+(X^1\Sigma^+, v^+) + N(^2P) \\ \rightarrow {}^2\Sigma^- \text{or} {}^2\Delta \rightarrow NO^+(X^1\Sigma^+, v^+) + N(^2D) \end{cases}. \quad (6)$$

The lifetime of 3×10^{-14} s was obtained for the $B^2\Pi$ state in a recent ion–electron velocity vector correlation measurement,[49] and the previous calculation[3] suggested that the $B^2\Pi$ state can readily dissociate via the conical intersection of its $^2A''$ component with the $^2\Sigma^-$ or $^2\Delta$ states. Thus the interaction between the $C^2\Sigma^+$ and $B^2\Pi$ states is just the rate-controlling step for the two dissociation pathways in Eq. (6), and the subsequent dissociation from the $B^2\Pi$ state is really rapider indeed, which is consistent with our conclusions in Sec. III D. In addition, since the bending of the $N_2O^+(B^2\Pi)$ ion was suggested to occur prior to dissociation,[49] the high J rotational excitation is expected, and hence, individual vibrational state of the NO^+ fragment is difficult to be identified clearly in our images due to overlapping of rotational contour.

Interestingly, different from the previous conclusion,[34] the internal state distributions along the $NO^+(X^1\Sigma^+) + N(^2D)$ and $NO^+(X^1\Sigma^+) + N(^2P)$ dissociation channels exhibit some dependence with the excited vibrational mode for $N_2O^+(C^2\Sigma^+)$, as shown in Fig. 3. Since two distributions have very similar profiles, the branching ratio along two channels can be estimated roughly using the intensities of their distribution peaks. For the (0,0,0) and (1,0,0) vibrational bands of $C^2\Sigma^+$ state, more than 73% NO^+ fragment is produced through the $NO^+(X^1\Sigma^+) + N(^2P)$ dissociation channel, while this ratio is obviously decreased to about 60% when the $v_3{}^+$ mode of the $C^2\Sigma^+$ state is excited. Therefore, the excited $v_3{}^+$ vibration seems beneficial to enhance the coupling between the $B^2\Pi$ and $^2\Sigma^-$ (or $^2\Delta$) states, according to the indirect predissociation mechanism. Previous theoretical calculation[3] shows that the N–N bond length of the $B^2\Pi$ geometry is much longer than that of the linear $C^2\Sigma^+$ state, and the $^2\Sigma^-$ and $^2\Delta$ states are repulsive along the N–NO distance. Consequently, the excitation of $v_3{}^+$ mode can potentially enhance the interaction between the $B^2\Pi$ state and the repulsive states $^2\Sigma^-$ (or $^2\Delta$), since the $v_3{}^+$ vibration of N_2O^+ is dominantly contributed by the N–N bond stretching. Unfortunately, in the case of lack of potential energy surfaces and related calculations of coupling, it is still a qualitative conclusion.

In the previous study,[34] the $NO^+(X^1\Sigma^+,v^+)$ ions were observed in the DPI process via $B^2\Pi$ state with vibrational excitation, mainly to $v^+ = 3$. More interestingly, as the photon energy increases much along the B state, the KERD of NO^+ almost remains fixed, and the vibrational distribution of $NO^+(X^1\Sigma^+,v^+)$ extends from $v^+ = 0$ to 6, with a maximum intensity at $v^+ = 4$.[49] Obviously, the vibrational populations of NO^+ observed in present experiments agree very well with the previous conclusion, which further supports the indirect predissociation mechanism via $B^2\Pi$. As mentioned above, the rate-controlling steps for both dissociation channels are of the same crossing from $C^2\Sigma^+$ to $B^2\Pi$. Therefore, the final vibrational populations of NO^+ fragments should be mainly determined by the dissociative behavior of the intermediate $B^2\Pi$ state. Because of the quasicontinuum dissociation of $B^2\Pi$, the most dominant vibronic distribution of NO^+ should correlate to the maximum overlap of the wave functions of $B^2\Pi$ and different v^+ dissociation channels. However, it is really a difficult work because the bending motion should be involved as Lebech *et al.* suggested.[35]

IV. CONCLUSION

Using synchrotron radiation as light source and the novel TPEPICO velocity imaging technique, the DPI process of the N_2O molecule in the excitation energy range of 19.9–21.0 eV has been detailedly investigated. Four fragment ions, NO^+, $N_2{}^+$, O^+, and N^+, are observed in the TPEPICO TOF-MS of the $N_2O^+(C^2\Sigma^+)$ state, respectively. Consequently, the branching ratios of different ions are estimated, and the NO^+ and N^+ are always dominant in the whole energy range.

The TPEPICO 3D time-sliced velocity images have been recorded for NO^+ fragment ions dissociated from various vibrational state-selected $N_2O^+(C^2\Sigma^+)$ ions, e.g., (0,0,0), (1,0,0), and (0,0,1). The kinetic and internal energy distributions of NO^+ fragments have been obtained directly from these images as the typical bimodal distributions, suggesting that the NO^+ fragments are formed via both $NO^+(X^1\Sigma^+) + N(^2P)$ and $NO^+(X^1\Sigma^+) + N(^2D)$ dissociation channels. On the contrary, the lowest dissociation channel, $NO^+(X^1\Sigma^+) + N(^4S)$, is negligible in dissociation of the $C^2\Sigma^+$ state, which is totally different from the predissociation of the $A^2\Sigma^+$ state, although both the electronic states have the same symmetry and very similar geometries. With the aid of theoretical potential energy surfaces of the lower lying electronic states of N_2O^+, the interaction between the $B^2\Pi$ and $C^2\Sigma^+$ states is the unique mechanism to cause the predissociation of $N_2O^+(C^2\Sigma^+)$ to form $N(^2P)$ and $NO^+(X^1\Sigma^+)$ fragments. Consequently, the $N(^2D)$ formation is caused by an indirect predissociation of $N_2O^+(C^2\Sigma^+) \rightarrow N_2O^+(B^2\Pi) \rightarrow N_2O^+(^2\Sigma^-$ or $^2\Delta) \rightarrow NO^+(X^1\Sigma^+) + N(^2D)$.

Based on the obtained KERD of NO^+ fragment, the very similar vibrational population reversions are identified for

both dissociation pathways. Interestingly, the obtained distributions of NO^+ fragments for both dissociation channels exhibit some dependence on the excited vibrational mode of $N_2O^+(C^2\Sigma^+)$, in which the excited v_3^+ asymmetrical stretching vibration can effectively promote dissociation possibility along the $NO^+(X^1\Sigma^+) + N(^2D)$ pathway. In addition, all the anisotropic parameters of NO^+ dissociated from the $N_2O^+(C^2\Sigma^+)$ ions have also been obtained to be close to 0.5. Therefore, the $C^2\Sigma^+$ state of N_2O^+ is fully predissociative indeed with a tendency of parallel dissociation, which is consistent with previous conclusions.[35]

ACKNOWLEDGMENTS

We would like to thank the financial support from the National Natural Science Foundation of China (NSFC, Nos. 10979042 and 21027005) and National Key Basic Research Special Foundation (NKBRSF, Nos. 2007CB815204 and 2010CB923300). X. Zhou also thanks the Fundamental Research Funds for the Central Universities for the support.

[1] D. G. Hopper, J. Am. Chem. Soc. **100**, 1019 (1978).
[2] X. Li, Y. L. Huang, G. D. Flesch, and C. Y. Ng, J. Chem. Phys. **106**, 1373 (1997).
[3] G. Chambaud, H. Gritli, P. Rosmus, H. J. Werner, and P. J. Knowles, Mol. Phys. **98**, 1793 (2000).
[4] J. W. Duff and D. R. Smith, J. Atmos. Sol.-Terr. Phys. **62**, 1199 (2000).
[5] J. L. Le Garrec, S. Carles, T. Speck, J. B. A. Mitchell, B. R. Rowe, and E. E. Ferguson, Chem. Phys. Lett. **372**, 485 (2003).
[6] J. C. Lorquet and C. Cadet, Int. J. Mass Spectrom. Ion Phys. **7**, 245 (1971).
[7] S. D. Peyerimhoff and R. J. Buenker, J. Chem. Phys. **49**, 2473 (1968).
[8] C. R. Brundle and D. W. Turner, Int. J. Mass Spectrom. Ion Phys. **2**, 195 (1969).
[9] D. W. Turner and D. P. May, J. Chem. Phys. **46**, 1156 (1967).
[10] M. J. Weiss, Chem. Phys. Lett. **39**, 250 (1976).
[11] P. M. Dehmer, J. L. Dehmer, and W. A. Chupka, J. Chem. Phys. **73**, 126 (1980).
[12] R. Locht, G. Caprace, and J. Momigny, Chem. Phys. Lett. **111**, 560 (1984).
[13] I. Nenner, P. M. Guyon, T. Baer, and T. R. Govers, J. Chem. Phys. **72**, 6587 (1980).
[14] M. Richard-Viard, A. Delboulbe, and M. Vervloet, Chem. Phys. **209**, 159 (1996).
[15] M. Richard-Viard, O. Atabek, O. Dutuit, and P. M. Guyon, J. Chem. Phys. **93**, 8881 (1990).
[16] S. Y. Chiang and C. I. Ma, J. Phys. Chem. A **104**, 1991 (2000).
[17] R. T. Wiedmann, E. R. Grant, R. G. Tonkyn, and M. G. White, J. Chem. Phys. **95**, 746 (1991).
[18] W. Kong, D. Rodgers, and J. W. Hepburn, Chem. Phys. Lett. **221**, 301 (1994).
[19] W. W. Chen, J. B. Liu, and C. Y. Ng, J. Phys. Chem. A **107**, 8086 (2003).
[20] J. M. Hollas and T. A. Sutherley, Chem. Phys. Lett. **21**, 167 (1973).
[21] H. Koppel, L. S. Cederbaum, and W. Domcke, Chem. Phys. **69**, 175 (1982).
[22] J. L. Olivier, R. Locht, and J. Momigny, Chem. Phys. **68**, 201 (1982).
[23] J. L. Olivier, R. Locht, and J. Momigny, Chem. Phys. **84**, 295 (1984).
[24] R. Locht, G. Hagenow, K. Hottmann, and H. Baumgartel, Chem. Phys. **151**, 137 (1991).
[25] H. F. Xu, Y. Guo, Q. F. Li, S. L. Liu, X. X. Ma, J. Liang, and H. Y. Li, J. Chem. Phys. **119**, 11609 (2003).
[26] H. F. Xu, Y. Guo, Q. F. Li, Y. Shi, S. L. Liu, and X. X. Ma, J. Chem. Phys. **121**, 3069 (2004).
[27] H. F. Xu, Y. Guo, Q. F. Li, J. H. Dai, S. L. Liu, X. X. Ma, J. Liang, and H. Y. Li, Acta Phys. Sin. **53**, 1027 (2004).
[28] H. Wang, X. G. Zhou, S. L. Liu, B. Jiang, D. X. Dai, and X. M. Yang, J. Chem. Phys. **132**, 244309 (2010).
[29] P. Coppens, J. Smets, M. G. Fishel, and J. Drowart, Int. J. Mass Spectrom. Ion Phys. **14**, 57 (1974).
[30] J. Berkowitz and J. H. D. Eland, J. Chem. Phys. **67**, 2740 (1977).
[31] S. Abed, M. Broyer, M. Carre, M. L. Gaillard, and M. Larzilliere, Chem. Phys. **74**, 97 (1983).
[32] M. Larzilliere and C. Jungen, Mol. Phys. **67**, 807 (1989).
[33] J. H. D. Eland, Int. J. Mass Spectrom. Ion Phys. **12**, 389 (1973).
[34] E. Kinmond, J. H. D. Eland, and L. Karlsson, Int. J. Mass Spectrom. **185/186/187**, 437 (1999).
[35] M. Lebech, J. C. Houver, D. Dowek, and R. R. Lucchese, J. Chem. Phys. **117**, 9248 (2002).
[36] X. F. Tang, X. G. Zhou, M. L. Niu, S. L. Liu, J. D. Sun, X. B. Shan, F. Y. Liu, and L. S. Sheng, Rev. Sci. Instrum. **80**, 113101 (2009).
[37] T. Baer, *Gas Phase Ion Chemistry* (Academic, New York, 1979), Vol. **1**, p. 153.
[38] T. Baer and Y. Li, Int. J. Mass Spectrom. **219**, 381 (2002).
[39] A. Eppink and D. H. Parker, Rev. Sci. Instrum. **68**, 3477 (1997).
[40] S. S. Wang, R. H. Kong, X. B. Shan, Y. W. Zhang, L. S. Sheng, Z. Y. Wang, L. Q. Hao, and S. K. Zhou, J. Synchrotron Radiat. **13**, 415 (2006).
[41] D. Townsend, M. P. Minitti, and A. G. Suits, Rev. Sci. Instrum. **74**, 2530 (2003).
[42] Y. Shi, Q. F. Li, H. Wang, J. H. Dai, S. L. Liu, and X. X. Ma, Acta Phys. Sin. **54**, 2418 (2005).
[43] D. P. Seccombe, R. Y. L. Chim, G. K. Jarvis, and R. P. Tuckett, Phys. Chem. Chem. Phys. **2**, 769 (2000).
[44] K. M. Weitzel and J. Mahnert, Int. J. Mass Spectrom. **214**, 175 (2002).
[45] See supplementary material at http://dx.doi.org/10.1063/1.3549130 for the image disposure scheme used in present experiments.
[46] J. E. Bartmess, *NIST Chemistry WebBook* (NIST, Gaithersburg, 2005).
[47] J. A. Coxon, M. A. A. Clyne, and D. W. Setser, Chem. Phys. **7**, 255 (1975).
[48] R. N. Zare, Mol. Photochem. **4**, 1 (1972).
[49] M. Lebech, J. C. Houver, D. Dowek, and R. R. Lucchese, J. Chem. Phys. **120**, 8226 (2004).